

Cite this article as: Li Minmin, Zuo Jianhua, Hou Yongjie, et al. Interaction and Magnetic Properties of NdCeFeB Melt-Spun Ribbons[J]. Rare Metal Materials and Engineering, 2023, 52(08): 2732-2736.

ARTICLE

Interaction and Magnetic Properties of NdCeFeB Melt-Spun Ribbons

Li Minmin¹, Zuo Jianhua¹, Hou Yongjie¹, Bo Yu¹, Zhang Ming¹, Dong Fuhai¹, Li Zhi¹, Liu Fei¹, Liu Yanli¹, Bai Suo¹, Li Zhubai¹, Li Yongfeng^{1,2}

¹School of Science, Inner Mongolia University of Science and Technology, Baotou 014010, China; ²Instrumental Analysis Center, Inner Mongolia University of Science and Technology, Baotou 014010, China

Abstract: The alloy ingots with nominal compositions of $(\text{Nd}_{1-x}\text{Ce}_x)_{2.4}\text{Fe}_{14}\text{B}$ ($x=0, 0.2, 0.4, 0.6, 0.8, 1.0$) were prepared by induction melting and then melt-spun to form nanocrystalline ribbons. Phase composition, magnetic properties and microstructure were investigated. XRD results show that all melt-spun ribbons exhibit the tetragonal structure $(\text{Nd,Ce})_2\text{Fe}_{14}\text{B}$ phase. When Ce substitution content is more than $x=0.6$, CeFe_2 phase appears and CeFe_2 content increases with the increase in Ce substitution content. Remanence, remanence ratio (M_r/M_s) and lattice constant decrease while increasing Ce substitution content. A coercivity of 1.31×10^6 A/m and the maximum energy product of 103 kJ/m^3 for $(\text{Nd}_{0.8}\text{Ce}_{0.2})_{2.4}\text{Fe}_{14}\text{B}$ melt-spun ribbon are achieved. The coercivity mechanism and intergrain exchange coupling were studied. The positive δM value was observed in every sample, confirming the existence of exchange coupling interaction. The δM maximum value reaches 0.76 at the Ce substitution content $x=0.2$, indicating that the intergranular exchange coupling effect is the strongest, which is consistent with the varying remanence ratio. SEM observation reveals that increasing Ce substitution deteriorates the columnar crystal structure of ribbons.

Key words: NdCeFeB; melt-spun ribbons; microstructure; interaction; magnetic properties

NdFeB magnets are the most widely used permanent magnets due to the outstanding magnetic performance, which strongly rely on the rare earth elements such as Nd, Dy, Pr and Tb^[1-3]. Recently, partly substitution Ce for Nd has attracted more attention because Ce is the most abundant and cheap rare earth element, it cannot only reduce the cost of NdFeB magnets but also balance the utilization of rare earth resources^[4-5]. It has been proved that Ce can restrain grain growth and modify microstructure, which can effectively inhibit the deterioration of magnetic properties when Ce substitution is less than 30wt% of total amount of rare earth^[6-7]. According to Ref.[8-11], the coercivity of Nd-Ce-Fe-B melt-spun ribbons abnormally increases when Ce substitution is around 20wt% , leading to a structural instability according to simulation result^[12-13]; the scattering lattice constant and the change of the Ce valence state are also the direct reason for the abnormal increase^[14]. It has been shown that when increasing the Ce substitution content, the

magnetic properties of $\text{Nd}_{12-x}\text{Ce}_x\text{Fe}_{82}\text{B}_6$ melt-spun ribbons decrease monotonously^[15]. Yang^[14] tested the recoil loops of $(\text{Nd}_{1-x}\text{Ce}_x)_{31.5}\text{Fe}_{67.5}\text{B}_1$ melt-spun ribbons, and the results showed that the recoil loop is fully closed at $x=0.2$ and the ribbon has a better resistance to reverse magnetic field, suggesting that the magnetic properties are better than those of others. The above results all discussed the effects of Ce substitution on the microstructures and magnetic properties of nanocrystalline Nd-Ce-Fe-B ribbons. However, there are relatively few reports on the coercivity mechanism of nanocrystalline Nd-Ce-Fe-B ribbons. In this work, nanocrystalline $(\text{Nd}_{1-x}\text{Ce}_x)_{2.4}\text{Fe}_{14}\text{B}$ melt-spun ribbons were prepared and investigated in order to explore the influence of Ce content on magnetic properties and coercivity mechanism of Nd-Ce-Fe-B melt spun ribbons.

1 Experiment

The alloy ingots with nominal compositions of $(\text{Nd}_{1-x}\text{Ce}_x)_{2.4}\text{Fe}_{14}\text{B}$ ($x=0, 0.2, 0.4, 0.6, 0.8, 1.0$) were prepared by induction

Received date: February 19, 2023

Foundation item: National Key Research and Development Program of China (2022YFB3505800); National Natural Science Foundation of China (51761031, 51961031); Natural Science Foundation of Inner Mongolia Autonomous Region (2019MS05040)

Corresponding author: Zuo Jianhua, Ph. D., School of Science, Inner Mongolia University of Science and Technology, Baotou 014010, P. R. China, E-mail: zuojianhua@imust.edu.cn

Copyright © 2023, Northwest Institute for Nonferrous Metal Research. Published by Science Press. All rights reserved.

melting. Excess Nd and Ce of 5wt% were added to compensate the mass loss due to evaporation. Each ingot was melt for three times to ensure the homogeneity. The ribbons were obtained directly by induction melting the precursor ingot in a quartz tube, and then ejected onto a surface of a copper wheel with a speed of 10–40 m/s. Then the ribbons were ground into powder and then examined by X-ray diffraction (XRD) with Cu K α radiation to determine the crystal structure. The magnetic hysteresis loops at room temperature were measured by vibrating sample magnetometer (VSM) with a maximum magnetic field of 2.39×10^6 A/m. The applied field is parallel to the plane of ribbons and no demagnetization correction for the geometry of the sample was made.

2 Results and Discussion

For ribbons prepared by melt-spinning, magnetic properties are strongly dependent on the wheel velocity. Fig.1 shows the hysteresis loops (Fig. 1a) and magnetic properties (Fig. 1b) of $(\text{Nd}_{1-x}\text{Ce}_x)_{2.4}\text{Fe}_{14}\text{B}$ ($x=0, 0.2, 0.4, 0.6, 0.8, 1.0$) ribbons prepared at optimum wheel speed. The single hard magnetic phase behavior is shown in melt-spun ribbons; the squareness of hysteresis loop becomes poorer when Ce substitution exceeds $x=0.2$. With increasing Ce substitution content, the coercivity decreases monotonically. Since the magnetocrystalline anisotropy of $\text{Ce}_2\text{Fe}_{14}\text{B}$ is lower than that of $\text{Nd}_2\text{Fe}_{14}\text{B}$ ^[16], the substitution by Ce decreases the magnetocrystalline anisotropy of $(\text{Nd}_{1-x}\text{Ce}_x)_{2.4}\text{Fe}_{14}\text{B}$, which should be responsible for the decrease in coercivity. Moreover, the coercivity values are consistent with the previous study from Hono^[17] and the

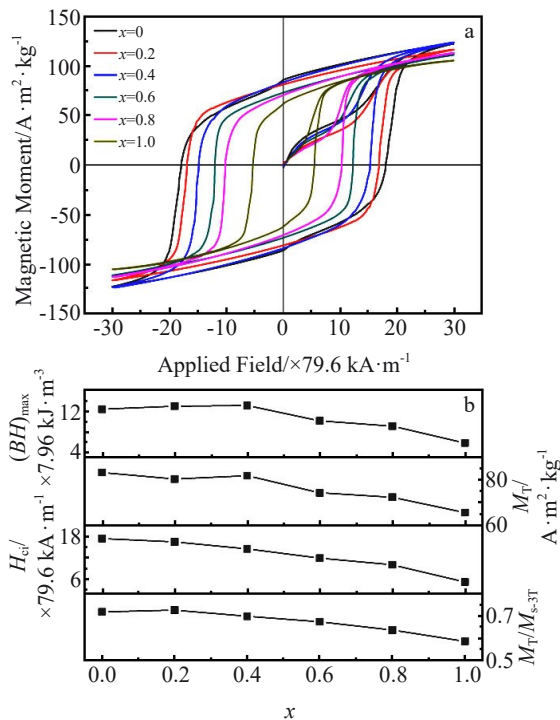


Fig.1 Hysteresis loops (a) and magnetic properties (b) of $(\text{Nd}_{1-x}\text{Ce}_x)_{2.4}\text{Fe}_{14}\text{B}$ ribbons

typical coercivity values reported for Nd-Fe-B-based melt-spun ribbons are 0.8–2.3 T. The change in remanence of the ribbons is fluctuant, and at the substitution content of $x=0.4$, the remanence is a little higher than that at $x=0.2$. Besides, the maximum energy product of ribbons slightly increases first when the substitution content is no more than $x=0.4$, and significantly decreases with increase in Ce substitution content. When Ce substitution content is $x=0.2$, the ribbon reaches the optimal performance: $H_{ci}=1.31 \times 10^6$ A/m, $(BH)_{\text{max}}=103 \text{ kJ/m}^3$. The value of remanence ratio M_r/M_s of an isotropic magnet composed of uniaxial anisotropy single-domain grains without intergrain interaction is 0.5, as seen in Fig. 1b, due to the nanoscale grain size, the values of remanence ratio M_r/M_s are all over 0.5 and peaks appear at Ce substitution of $x=0.2$, which indicates that the intergranular exchange coupling interaction is strong in $(\text{Nd}_{1-x}\text{Ce}_x)_{2.4}\text{Fe}_{14}\text{B}$ melt spun ribbons. The change of remanence ratio affects the change of the maximum energy product.

Fig.2 shows the XRD patterns of prepared $(\text{Nd}_{1-x}\text{Ce}_x)_{2.4}\text{Fe}_{14}\text{B}$ ribbon powders. Obviously, only $(\text{Nd,Ce})_2\text{Fe}_{14}\text{B}$ phase and CeFe_2 phase emerge in the XRD patterns, no other phases are present, and no Nd-rich phase and α -Fe are found. When the ribbon does not contain Ce ($x=0$) and Ce substitution is small ($x=0.2, 0.4$), XRD patterns confirm that $(\text{Nd,Ce})_2\text{Fe}_{14}\text{B}$ phase is the dominant phase; diffraction patterns of CeFe_2 phase appear when the Ce substitution content is higher ($x=0.6, 0.8, 1.0$) and the intensity increases with increasing Ce substitution content, which means that the content of CeFe_2 phase increases. The CeFe_2 contents at $x=0.8$ and $x=1.0$ are 3.6% and 9.6%, respectively. The CeFe_2 phase is paramagnetic at room temperature, and has a smaller magnetic moment compared to $(\text{Nd,Ce})_2\text{Fe}_{14}\text{B}$ phase. CeFe_2 content increases with increasing Ce substitution content, which reduces the magnetic properties of the ribbons as shown in Fig. 1. Previous studies have shown that the CeFe_2 phase in the magnet is inevitable when the cerium content is high which is generally considered to be harmful to the performance of magnets^[18]. The appearance of CeFe_2 phase and the increasing content CeFe_2 phase with Ce substitution are another main reason for the change of magnetic properties. In addition, as the Ce substitution content increases, the XRD peaks shift to higher

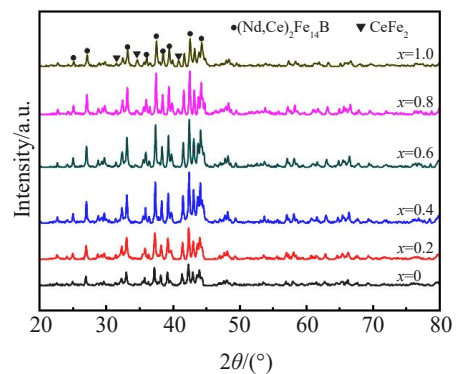


Fig.2 XRD patterns of $(\text{Nd}_{1-x}\text{Ce}_x)_{2.4}\text{Fe}_{14}\text{B}$ ribbons powder

degree because the Ce atomic radius is smaller than Nd atomic radius, which indicates that the lattice constants decrease. The lattice constants calculated from XRD data are summarized in Fig.3. It can be seen that the lattice constants and cell volume decrease while increasing the substitution content. The grain size of melt-spun ribbons with different Ce substitution contents was calculated based on Scherrer formula, and the average grain sizes are 49, 43, 46, 47, 49 and 54 nm at $x=0, 0.2, 0.4, 0.6, 0.8, 1.0$, respectively, as shown in Fig.3. The average grain size varies with the change in Ce content, it is the lowest at $x=0.2$, and then increases with the increase in Ce substitution content. Zha^[5] found the same grain size variation trend in the $(\text{Nd}_{1-x}\text{Ce}_x)_{12.2}\text{Fe}_{81.6}\text{B}_{6.2}$ melt-spun ribbons.

As Ce-substituted ribbons have shown significant effects on structure and magnetic properties, their microstructure was analyzed by SEM (Fig.4). It can be clearly seen that the free side of the ribbons is composed of columnar grains; there is a significant difference for these samples. With Ce substitution for Nd by 20%, the columnar grains are finer and uniform; but for other composite samples, columnar grains vary, and some grains are coarse, the microscopic morphology is deteriorated.

Minor hysteresis loops were used to investigate the coercivity mechanism of $(\text{Nd}_{1-x}\text{Ce}_x)_{2.4}\text{Fe}_{14}\text{B}$ ribbons. Fig. 5 reveals the dependence of normalized coercivity and remanence in minor loops on the applied field. The inset is the original minor loops measured by VSM. Asymmetric minor loops are observed when the maximum applied field for certain minor loops is lower than the intrinsic coercivity. This phenomenon may be resulted from the pinning effect of domain wall movements during the magnetization process. The normalized coercivity and remanence increase slowly when the applied magnetic field is lower than the coercivity of ribbon. The normalized coercivity increases faster than remanence, which is another evidence for the dominant role of pinning mechanism on the coercivity of ribbons.

To investigate the exchange coupling between the grains, Henkel plot was measured for all samples, which can be defined as $\delta M = [2M_r(H) + M_d(H)]/M_r - 1$ ^[19], where $M_r(H)$ is the remanence obtained after the application and subsequent

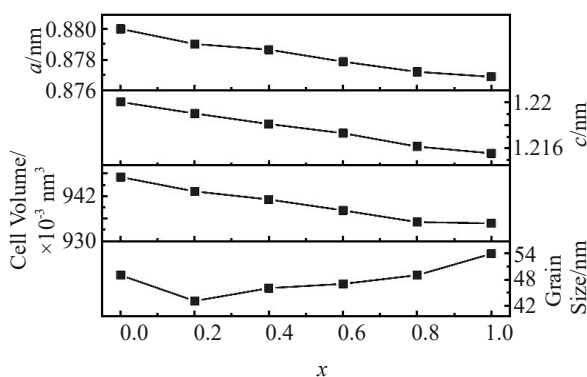


Fig.3 Lattice constants and grain size of $(\text{Nd}_{1-x}\text{Ce}_x)_{2.4}\text{Fe}_{14}\text{B}$ ribbons powder

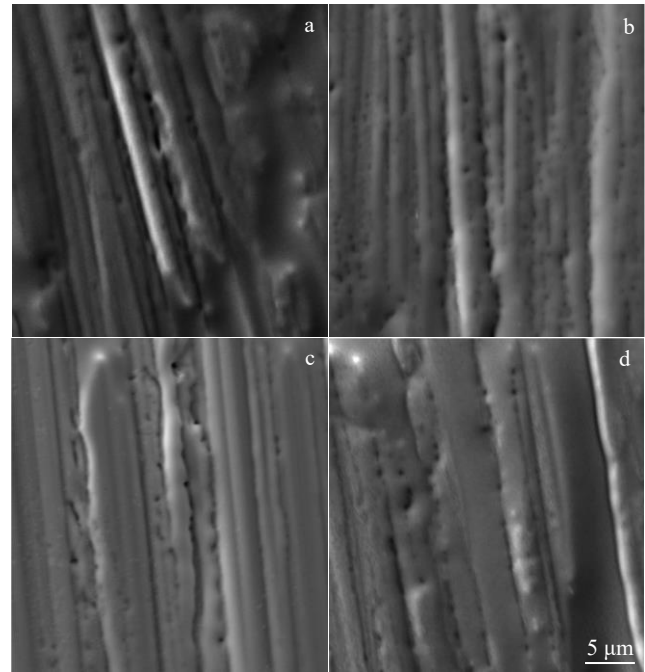


Fig.4 SEM images of free-side of $(\text{Nd}_{1-x}\text{Ce}_x)_{2.4}\text{Fe}_{14}\text{B}$ ribbons: (a) $x=0$, (b) $x=0.2$, (c) $x=0.8$, and (d) $x=1.0$

elimination of the applied field H on the thermally demagnetized samples. $M_d(H)$ is obtained after saturation in one direction and a subsequent application and removal of a field H in the reverse direction, and M_r is the remanence for the sample magnetized to saturation. When the value of δM is positive, the exchange coupling interaction plays a main role, which indicates that grain interaction promotes magnetization state. When the value of δM is negative, the long-range magnetostatic interaction is relatively stronger, which indicates that grain interaction enhances the demagnetization effect. According to the Wohlfarth's analysis, the large amplitude of δM peak reflects the stronger intergranular action among grains. The fields corresponding to the peak of positive δM are comparable to the H_c of samples. Fig.6 displays the δM values of $(\text{Nd}_{1-x}\text{Ce}_x)_{2.4}\text{Fe}_{14}\text{B}$ ribbons. Different maximum values show the difference in intergrain interaction among samples, and with increasing the Ce substitution content, the positive and negative δM value gradually decreases. Positive maximum values of δM are observed for all ribbons at the field around coercivity, indicating that the exchange coupling is very strong in all these nanoscale ribbons, which should be partially responsible for the high remanence ratio for these samples. The values of δM for Nd-Ce-Fe-B ribbons are higher than that for Ce-Fe-B ribbon, and lower than that for Nd-Fe-B ribbon, and δM maximum value reaches 0.76 at $x=0.2$. The variation of δM is consistent with the variation of grain size, and the fine grain sizes promote the exchange coupling between grains. As the substitution content increases, the grain size gradually increases, the exchange coupling decreases and the long-range magnetostatic interaction becomes stronger and the dipolar interactions

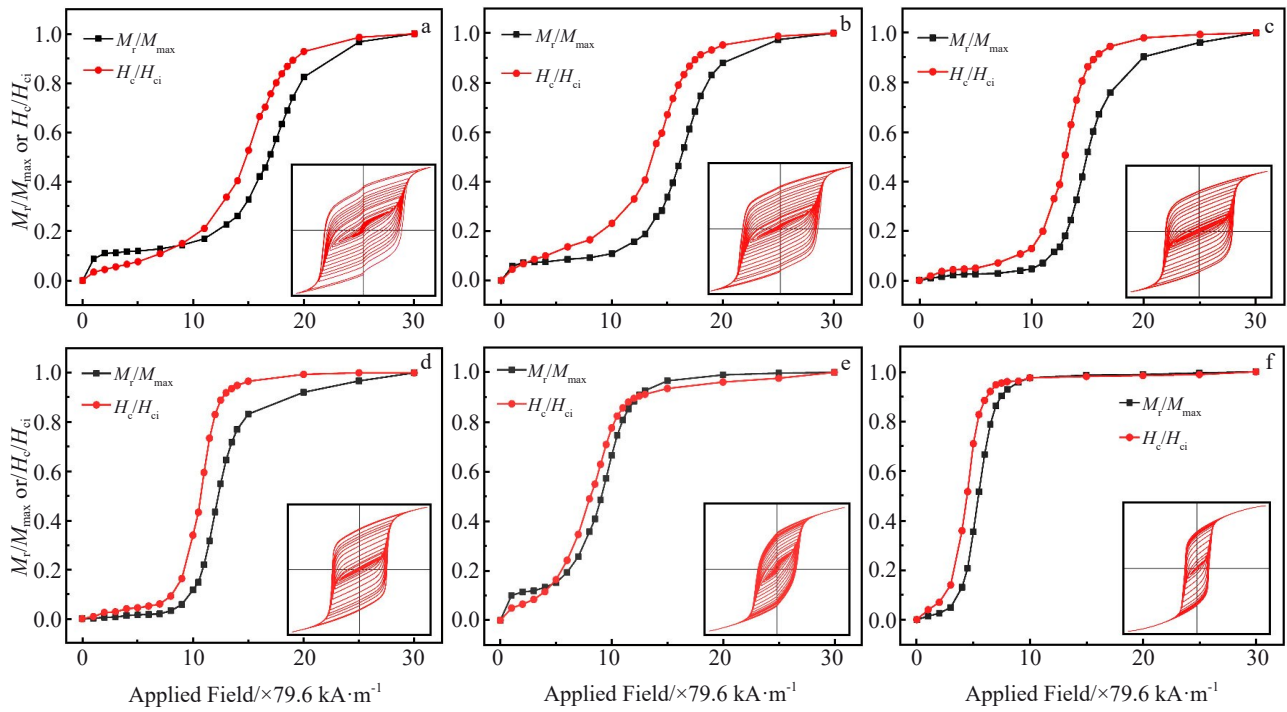


Fig.5 Dependence of H_c and B_r on applied field in minor loops of $(\text{Nd}_{1-x}\text{Ce}_x)_{2.4}\text{Fe}_{14}\text{B}$ ribbons: (a) $x=0$, (b) $x=0.2$, (c) $x=0.4$, (d) $x=0.6$, (e) $x=0.8$, and (f) $x=1.0$

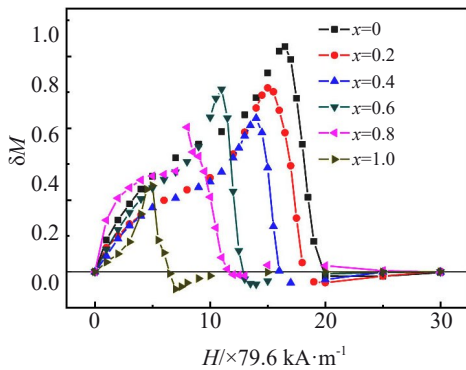


Fig.6 Henkel plots of $(\text{Nd}_{1-x}\text{Ce}_x)_{2.4}\text{Fe}_{14}\text{B}$ ribbons

appears. The interaction for Nd-Ce-Fe-B alloy will be further investigated.

3 Conclusions

Phase composition and magnetization reversal behavior of nanocrystalline $(\text{Nd}_{1-x}\text{Ce}_x)_{2.4}\text{Fe}_{14}\text{B}$ ($x=0, 0.2, 0.4, 0.6, 0.8, 1.0$) melt-spun ribbons are investigated. The ribbons can crystallize in a tetragonal 2:14:1 structure. The high remanence ratio (greater than 0.5) indicates the strong exchange coupling interaction. The magnetization reversal behavior (δM plots) is taken into consideration. The positive δM values are observed in every sample, which confirms the existence of exchange coupling interaction. Evidently, a coercivity of 1.31×10^6 A/m, and the maximum energy product of 103 kJ/m^3 for $(\text{Nd}_{0.8}\text{Ce}_{0.2})_{2.4}\text{Fe}_{14}\text{B}$ melt-spun ribbon are achieved.

References

- 1 Fu S, Yan M, Jin J Y et al. *Materials Letters*[J], 2021, 283(15): 128-131
- 2 Wang Z J, Yue M, Liu W Q et al. *Scripta Materialia*[J], 2022, 217: 114-118
- 3 Song T T, Li X, Tang X et al. *Journal of Materials Science & Technology*[J], 2022, 122: 121
- 4 Song L W, Yu N J, Zhu M G et al. *Journal of Rare Earths*[J], 2018, 36: 95
- 5 Zha L, Liu Z, Chen H et al. *Journal of Rare Earths*[J], 2019, 37: 1053
- 6 Huang S L, Feng H B, Zhu M G et al. *International Journal of Minerals Metallurgy Materials*[J], 2015, 22: 417
- 7 Yan C J, Guo S, Chen R J et al. *IEEE Transactions on Magnetics* [J], 2014, 50: 2102-2105
- 8 Pathak A K, Mahmud K, Gschneidner K A et al. *Advanced Materials* [J], 2015, 27: 2663
- 9 Hussain M, Zhao L Z, Zhang C et al. *Physica B: Condensed Matter*[J], 2016, 483: 69
- 10 Tang X, Song S Y, Li J et al. *Acta Materialia*[J], 2020, 190: 8
- 11 Wang Y L, Zhang G Q, Huang Y L et al. *Rare Metal Materials and Engineering* [J], 2018, 47(1): 5
- 12 Alam A, Johnson D D. *Physical Review B*[J], 2014, 89: 235-236
- 13 Alam A, Khan M, McCalum R W et al. *Applied Physics Letters*[J], 2013, 102: 42-402
- 14 Yang M N, Wang H, Hu Y F et al. *Journal of Alloys and Compounds* [J], 2017, 710: 519

- 15 Li Z B, Shen B G, Zhang M et al. *Journal of Alloys and Compounds*[J], 2015, 628: 325
- 16 Herbst J F. *Reviews of Modern Physics*[J], 1991, 63: 819
- 17 Hono K, Sepehri-Amin H. *Scripta Materialia*[J], 2012, 67: 530
- 18 Zhang M, Li Z B, Shen B G et al. *Journal of Alloys and Compounds*[J], 2015, 651: 144
- 19 Wohlfarth E P. *Journal of Applied Physics*[J], 1958, 29: 595

NdCeFeB 快淬带相互作用与磁性能

李敏敏¹, 左建华¹, 侯永杰¹, 薄宇¹, 章明¹, 董福海¹, 李志¹, 刘飞¹, 刘艳丽¹, 白锁¹,
李柱柏¹, 李永峰^{1,2}

(1. 内蒙古科技大学理学院, 内蒙古包头 014010)

(2. 内蒙古科技大学分析测试中心, 内蒙古包头 014010)

摘要: 采用感应熔炼制备名义成分为 $(\text{Nd}_{1-x}\text{Ce}_x)_{2.4}\text{Fe}_{14}\text{B}$ ($x=0, 0.2, 0.4, 0.6, 0.8, 0.8, 1.0$)的快淬带, 研究了Ce取代量对快淬带的相组成、磁性能和微观结构的影响。XRD结果表明, 所有快淬带均呈现四方结构 $(\text{Nd, Ce})_2\text{Fe}_{14}\text{B}$ 相, 当Ce取代量超过 $x=0.6$ 时, 快淬带中出现 CeFe_2 相并且 CeFe_2 含量随着Ce取代量的增加而增加。快淬带的剩磁、剩磁比(M_r/M_s)和晶格常数随着Ce含量的增加而减小, 当Ce取代量为 $x=0.2$ 时, 快淬带的磁性能为矫顽力 1.31×10^6 A/m, 最大磁能积 103 kJ/m³。通过小回线和 δM 曲线研究了快淬带的矫顽力机理和晶粒间交换耦合, 在每个样品中都观察到正的 δM 值, 证实了交换耦合相互作用的存在。Ce含量为 $x=0.2$ 时 δM 最大值达到0.76, 说明快淬带晶粒间交换耦合效应最强, 这一结果与剩磁比的变化一致。SEM观察发现, Ce取代量的增加恶化快淬带的柱状晶结构。

关键词: NdCeFeB; 快淬带; 微观结构; 相互作用; 磁性能

作者简介: 李敏敏, 女, 1998年生, 硕士, 内蒙古科技大学理学院, 包头 内蒙古 014010, E-mail: MM-Lee1998@163.com